

Electrochemical and Corrosion Behavior of 2205 Duplex Stainless Steel in Simulated Concrete Pore Solution

Baosong Li^{1,*}, Weiwei Zhang²

¹ College of Mechanics and Materials, Hohai University, Nanjing 211100, China

² College of Mechanical and Electrical Engineering, Hohai University, Changzhou 213022, China

*E-mail: bsli@hhu.edu.cn

Received: 14 May 2017 / Accepted: 6 July 2017 / Published: 13 August 2017

In this paper, electrochemical and passivation behavior of 2205 duplex stainless steel (DSS) in simulated concrete pore solution (SCPS) under anoxic condition was studied. The electrochemical impedance spectroscopy (EIS) was mainly employed to evaluate the corrosion behavior of the passive film. The electrochemical behavior of DSS 2205 was investigated by potentiodynamic polarization, EIS, Mott-Schottky methods. The results show that the protective behavior of the passive film of DSS 2205 in SCPS at pH 12.5 is better than that of 13.3 and 13.8. The time for polarization current to reach an steady state will be prolonged with the pH value increase from 12.5 and be shorten as the formation potential increases. The passive film could display the behavior of both n-type and p-type semiconducting which is related to the formation potential. The optimal polarization potential for passivation of DSS 2205 in SCPS is related to the E_{corr} of the passive film, which is in the range of -400 mV to 0 mV.

Keywords: passivation; electrochemical impedance spectroscopy; 2205 duplex stainless steel; electrochemical behavior; simulated concrete pore solution

1. INTRODUCTION

In the past few years, the stainless steel is widely used to improve the corrosion resistance and extend the service life of the concrete construction [1, 2]. Due to the mixture of austenitic and ferritic phases, the duplex stainless steel (DSS), which has superior performances such as high strength, lower nickel content and excellent pitting corrosion resistance, is used as an alternative to traditional austenitic stainless steel in many fields [3, 4]. The corrosion resistance of the DSS 2205 is associated with the composition, microstructure, electrochemical or semiconductive behaviors of the passive film [5, 6]. The protective properties of the passive film is affected by various factors, such as the pH,

immersed time, polarization potential, dissolved oxygen and the interaction of multiple factors [7]. The concentration of chloride anions in the surroundings, pH and passive properties all play important roles in determining the metal corrosion susceptibility [8]. Till now, the corrosion of DSS 2205 reinforcement in concrete has already been studied much. However, present majority results, if not all, focused on the typical applied conditions [9, 10].

The composition of the concrete pore solution is very complex which has an important impact on the corrosion processes. We believed that the research of the corrosion behavior of steel in simple alkaline solution, such as saturated $\text{Ca}(\text{OH})_2$ solution, will contribute to a better understanding of the corrosion mechanism of embedded steels [11]. Till now, the electrochemical and passivation behavior of DSS 2205 combining in high alkaline ($\text{pH} > 12.5$) and anoxic environment at more negative polarization potential (-1.0 V-0 V) are scarcely investigated [12, 13]. The dynamic film formation process, the structure and properties of the passive film formed in the alkaline solution is still the unclear features to know [14, 15]. Due to the relatively low natural corrosion rate in concrete [16], till now, the electrochemical method is still a valuable tool for quick evaluation of steel reinforcement. Some in situ methods, including potentiodynamic polarization, cyclic voltammetry (CV), electrochemical impedance spectroscopy (EIS), capacitance measurements, have been employed to investigate the corrosion and passivation behavior of the passive films [17, 18]. Therefore, an attempt has been made in this paper to investigate the passivation of DSS 2205 in alkaline environment by the electrochemical technique.

The aim of this work is to investigate the accelerated passivation by potentiostatic polarization, to study the properties of DSS 2205 for better understanding the electrochemical behavior at more negative potential in alkaline and anoxic environment. Saturated calcium hydroxide solution with different pH by addition of sodium hydroxide, which was used as simulated concrete pore solution, has been employed as the high alkaline environment. EIS has been adopted as the primary tool for investigation the electrochemistry and corrosion behavior of DSS 2205 in SCPS solution.

2. EXPERIMENTAL

The chemical composition of DSS 2205 in weight percent was listed as follows: C 0.03, Mn 2.00, Si 1.00, p 0.03, S 0.02, Cr 22.0, Ni 5.5, Mo 3.18, N 0.16 and Fe balance. The specimen was machined and coupled to an insulated copper wire, then was cast in epoxy resin avoiding the presence of crevices. The exposed area was 1 cm^2 . Each specimen was mechanically abraded with successively 600, 800 and 1200 grit silicon carbide paper and rinsed with ethanol and double distilled water before the electrochemical measurement. Then, the electrode was immediately placed into the electrochemical cell. The N_2 deaerated saturated $\text{Ca}(\text{OH})_2$ solution with the pH adjusted to 12.5, 13.3 and 13.8 by addition of NaOH were named SCPS_{12.5}, SCPS_{13.3}, and SCPS_{13.8}, respectively. All chemicals employed were of analytical reagent grade. For each experiment, a newly polished specimen and a fresh solution has been used for each run.

All electrochemical experiments were performed in a three electrode cell by a Solartron 1280B electrochemical workstation. The sample was used as the working electrode, a platinum plate was used

as the counter electrode. A saturated calomel electrode (SCE) was used as the reference electrode. The solution was purged for 20 min before and during each experiment with high purity N_2 gas to simulate the anoxic conditions. Potentiodynamic polarization was performed at 0.1667 mV/s to determine the passive range. The polarization potential was then selected as the film formation potentials (from -800 mV to 0 mV with an interval of 100 mV) in the passive region. At each passive potential, potentiostatic polarization was kept for enough time (4 to 48 h) to ensure an “operational” steady state of the system. EIS was performed after potentiostatic polarization in an identical SCPS by scanning the frequency from the high (10000 Hz) to low (0.01 Hz) values and then immediately from low to high values.

3. RESULTS AND DISCUSSION

3.1 Potentiodynamic polarization and cyclic voltammetry behavior of DSS 2205

Fig.1a is the potentiodynamic scan plots of DSS 2205 in N_2 deaerated SCPS at different pH. As can be seen in Fig.1a, in the cathodic part, there are no obvious differences in the shape of the curves. While in the anodic region, passivation occurred in the range from -0.4 V to 0.47 V with several oxidation current peaks. It was observed that there was a sharp increase of the current density after 0.47 V which was the result of the breakdown of the passive film and oxygen evolution reaction. As seen in Fig.1a, it was observed that the DSS 2205 exhibited a stable passive range with the anodic oxidation peak at -0.45 V, -0.13 V and 0.45 V in the SCPS_{12.5}, which revealed that ferrous and chrome oxidation was taking place [19]. The E_{corr} positively shifts from -0.81 V in SCPS_{12.5} to -0.57 V in the SCPS_{13.3}. Four oxidation peaks were found corresponding to -0.43 V, -0.23 V, -0.01V, 0.4 V, respectively. When in SCPS_{13.8}, the E_{corr} positively shifts to -0.43 V, and there were three current peaks at -0.23 V, -0.1 V and 0.39 V. At potentials higher than 0.47 V, a sharp increase of the current density was observed. This is due to the onset of oxygen evolution reaction ($4\text{OH}^- \rightarrow \text{O}_2 + 2\text{H}_2\text{O} + 4e^-$), although passivity breakdown may occur simultaneously [20].

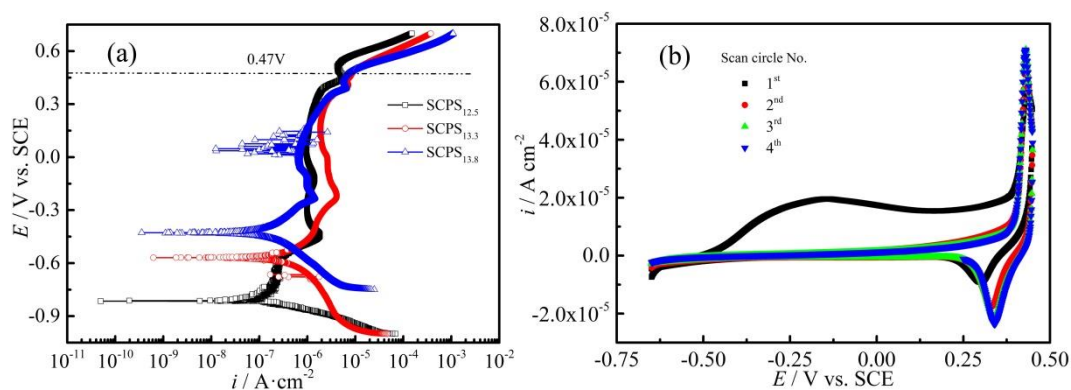


Figure 1. Potentiodynamic (a) and cyclic voltammetry (b) curves of DSS 2205 measured in the SCPS, 25°C, the scanning rate is 0.1667 mV/s for (a) and 5 mV/s for (b).

The cyclic voltammetry plots were also investigated as seen in Fig.1b. It can be seen that in the first scan cycle, a great oxidation peak was appeared in the positive scanning direction, which is associated with the formation of the passive films. However, in the next scanning cycle, the oxidation peak was disappeared. In the negative scan direction, the intensity of the reducing peak increases with the scan numbers. This indicates that a passive film was covered on the surface of DSS 2205 [21, 22]. In fact, the initial potential of passivity breakdown is usually negative than 0.47 V although the current has not increased much at that time. Subsequently, the dissolution rate of the passive film increases dramatically as the polarization potential is converted to the transpassive region. This process is related to the oxidative dissolution of the barrier films [23]. In addition, the E_{corr} of the DSS 2205 in different alkaline solution is varied and it takes long time to reach a steady state which will result in the deviation of the E_{corr} , especially for potentiodynamic polarization. In order to avoid the data deviation, consistent test conditions were employed, such as the same pretreatment, measure time, electrode system and configuration. Based on the Tafel curve, the passive film formation potentials (-700 mV to 0 mV with an interval of 100 mV) were opted for the potentiostatic polarization, covering the “lower” half of the passive region, to study the behavior of DSS 2205 at the very negative corrosion potential conditions.

3.2 Accelerated passivation of DSS 2205 via potentiostatic polarization

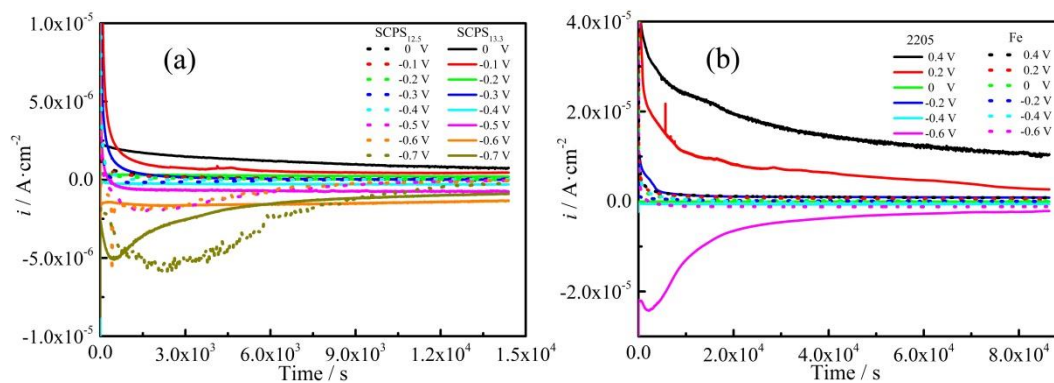


Figure 2. Traces of the current density passivated (a) 4 h, (b) 24 h at different polarization potential in (a) SCPS_{12.5} and SCPS_{13.3} for DSS 2205; (b) SCPS_{13.8} for DSS 2205 and 98% pure Fe.

The potentiostatic polarization was employed to accelerate the formation of passive film on DSS 2205 to reach an “operational” steady state. It should be pointed out that the E_{corr} of the passive steel is related to the structure and properties of the passive film, and varied at different environment [24]. This is associated with the passive film formed on the steel surface. Due to the difference of the passive film, the E_{corr} measured in the different stage of the passivation is corresponding to the different thickness of the passive film. It was known that the polarization current reflects the formation, early growth, depassivation and repassivation of the passive films [25]. Therefore, the traces of the current in the potentiostatic polarization process were recorded as shown in Fig.2. It is observed in Fig.2 that the net current density shifts to positive with the increase of the polarization potential. The

reason is probably that the thicker passive film was formed on the metal surface at higher potentials and less perturbation from the cathodic reaction, which increases exponentially with the decrease of the potential to more negative [26].

There are a few short-period current spikes, which are the results of the passivity breakdown followed immediately by repassivation [27]. This is probably associated with the impurity of the solution, especially the dissolved corrosion products of metallic ion. At SCPS_{13.8}, the current is higher than in the SCPS_{12.5}. The reason is that the corrosion or dissolution of passive film will be accelerated in the very alkaline environment. The time for polarization current to reach steady state (T_s) will be prolonged when the pH increases from 12.5 to 13.8. At higher alkaline environment, it takes longer time for the current to reach a steady state. This also certifies that it has deleterious effects on the formation of passive film in very alkaline solution. Moreover, as can be seen in Fig.2, on the whole, the T_s is short at high polarization potential and is long at low polarization potential. It also indicates that the pH value affects T_s in SCPS. It reveals that the very alkaline environment (pH >13) can delay the T_s of the formation of oxidation layer, in which process more time is needed for the current to reach stable. From above analysis, potentiostatic polarization 12 h to 36 h can achieve operational steady state of the passivation, which has greatly shortened the necessary time to reach the stable state of the passive film at free corrosion potential.

3.3 Electrochemical impedance spectroscopy behavior of DSS 2205

Due to its non-destructive property suitable for film corrosion monitoring [28], EIS was mainly employed to investigate the electrochemical properties of passive film. Fig.3 presents Nyquist and Bode plots of DSS 2205 after potentiostatic polarization 4 h at different potentials in SCPS at 25°C. It shows that the electrochemical impedance spectra in the N₂ deaerated SCPS solution were characterized by a capacitive semicircle arc covering most of the high-frequency region, which is attributed to the charge transfer process related to the film surface state. The Nyquist plots show the capacitive arc with different radii which has the typical form of the passive film. The similar shape of the plot shows that they have the similar corrosion mechanism. The high frequency semicircles are generally related to the charge transfer in the electrical double layer at the electrode passive film/electrolyte interface [29]. The radius indicates the polarization resistance of the charge transfer through the passive film [30]. The increase in the radius of the semicircle suggested an increase in the passive film stability. The small radius means the low resistance of the passive film [31, 32]. The appearance of the straight line shows that the kinetics of the dissolution of the oxide film is limited by diffusion of the oxidation products [33, 34].

As seen in Fig.3, the diameters of the capacitive loop decrease with the increase of pH from 12.5 (Fig.3a) to 13.3 (Fig.3b). The passive film of DSS 2205 in the SCPS_{12.5} solution is stable and has good corrosion resistance. The overall impedance shows higher values in SCPS_{12.5}, indicating that the corrosion resistance of the passive film is enhanced. The largest radius in SCPS_{12.5} is more than $4 \times 10^5 \Omega \cdot \text{cm}^2$. However, the radius decreases to $2 \times 10^5 \Omega \cdot \text{cm}^2$ in SCPS_{13.3}. It indicates that with the increase of the pH of the SCPS, the decrease in semicircle radius has demonstrated a decrease in the passive film

resistance with low stability. This suggests that very alkaline environment have deleterious effect on the passivation.

Polarization potential has a great influence on the passivation of DSS 2205 [35]. It can be seen in Fig.4 that when the potential is negative than -0.6 V, the radius of the capacitive semicircle is obviously small. In general, as the polarization potential becomes more positive (above -0.6V), the radius of the capacitive semicircle will increase, which implies the higher polarization resistance and better corrosion resistance provided by the oxide layer. However, the optimal potential for passivation of the DSS 2205 is also associated with the pH value of the SCPS. The highest polarization potential is not corresponding to the best impedance value. In the low alkaline environment, high potential is beneficial to generating more protective films. With the increase of pH from 12.5 to 13.8, it can be found that the best protective films will be formed at lower potential. The potential range of 300 mV positive to the passive film E_{corr} is believed the optimal polarization potential, which is usually in the range of -400 mV to 0 mV vs. SCE.

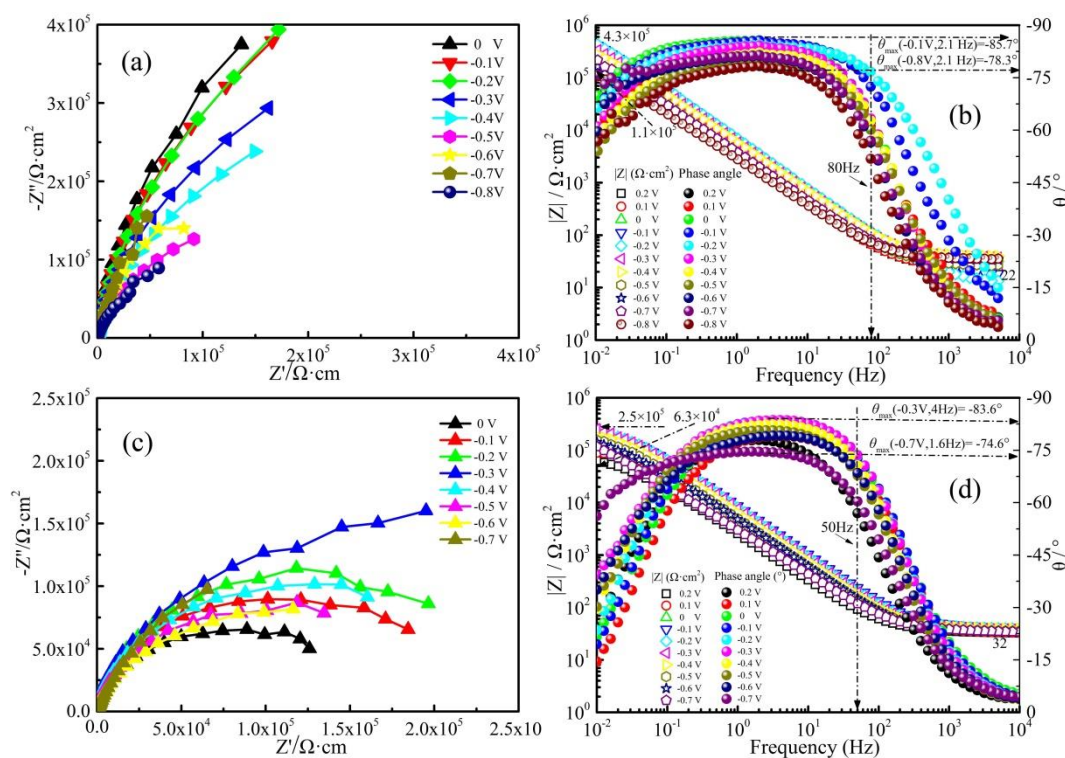


Figure 3. Nyquist and Bode plots of DSS 2205 passivated at different polarization potential for 4 h at 25°C in (a, b) SCPS_{12.5}, (c, d) SCPS_{13.3}.

Fig.3b and 3d shows the Bode plots of DSS 2205 after passivated 4 h at different polarization potential in SCPS. The bode plots of DSS 2205 show similar shapes and display the features of the passive metals. It is generally known that additional capacitance character can improve the protective ability of the passive film through hindering substance transportation across the film [36]. The modulus value and phase angle of the impedance are strongly influenced by the pH value and polarization potential. As can be seen in Fig.3b, with the increase of the polarization potential from -0.8 V to 0 V in

SCPS_{12.5}, the maximum of phase angle increases from -78.3° up to -85.7° in sequence. The modulus $|Z|$ at 0.01 Hz is $4.3 \times 10^5 \Omega \text{ cm}^2$. The maximum phase angle measured is around -85° over a wide range of frequencies, indicating a pure capacitive response. This is a typical impedance spectra when a stable passive film is formed on DSS 2205. This illustrates that the passive film within intermediate frequency range behaves similarly to a pure capacitor, which has a phase angle of -90° . This capacitive feature improves the stability of the protective passive film. As seen in Fig.3d, in SCPS_{13.3}, with the increase of the polarization potential from -0.7 V to -0.3 V , the maximum of phase angle increases from -74.6° up to -83.6° . This indicates that more protective passive films could be formed at more positive polarization potential in this potential region. However, in the low frequency range ($<1 \text{ Hz}$), the phase angle is lower compared with SCPS_{12.5} at the equal frequency. Also, it can be found that the modulus $|Z|$ at 0.01 Hz decreased to $2.5 \times 10^5 \Omega \text{ cm}^2$ which is smaller than $4.3 \times 10^5 \Omega \text{ cm}^2$ of Fig.3b.

Additionally, as for the formation potential, the phase angle value obviously decreased when the polarization potential is negative than -0.7 V vs. SCE. When the polarization potential is in the range of -0.6 V to 0 V , the passive film has the protective capacitive properties with the phase angle up to -84° . The increase of the impedance modulus of the film as the potential increases from -0.7 V is a result of the gradual thickening of the passive films and the development of the microstructure. It was believed that the larger impedance is attributed to the good passive film [37, 38]. Therefore, the reduction in impedance within transpassive region is associated with a loss of corrosion resistance of the passive film. In fact, transpassive dissolution of the oxide layer is closely related to the passivity breakdown.

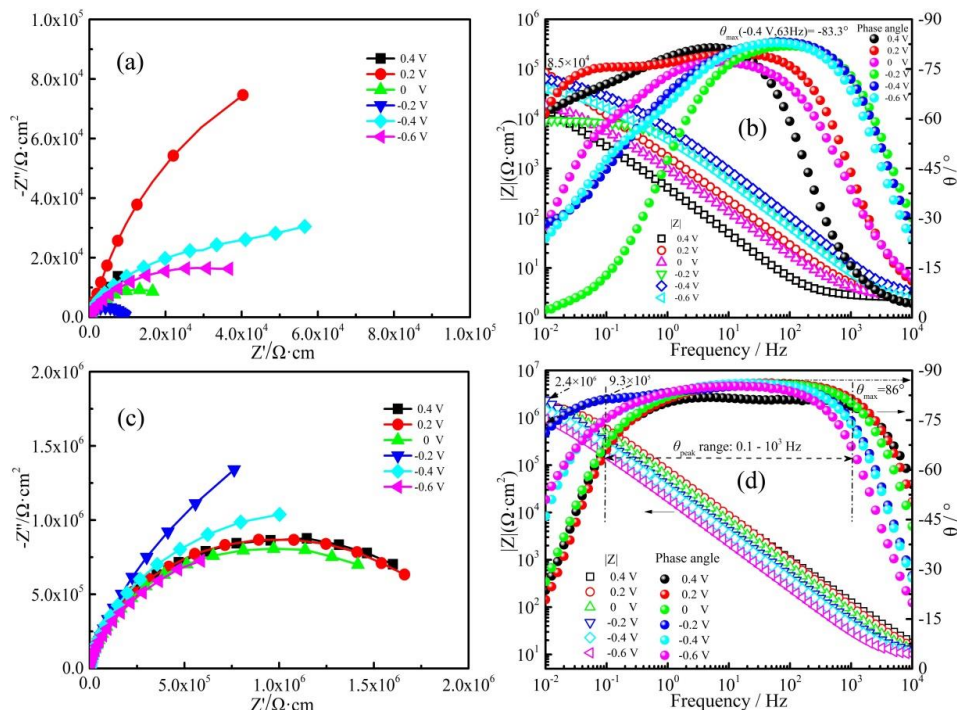


Figure 4. Nyquist and Bode plots of (a) DSS 2205 and (b) pure Fe passivated 24 h at different potential at 25°C in SCPS_{13.8}.

The electrochemical impedance spectra at higher alkaline environment of pH 13.8 can be seen in Fig.4. An interesting phenomenon was observed that at the polarization potential of -0.4 V, the maximum phase angle -83.3° was obtained. An important feature is that there was a second time constant which is related to the diffusion behavior of the corrosion products. The potential range of the phase angle peak shrank from low frequency range to intermedium frequency which is higher than 1 Hz. When the polarization potential is -0.6 V, the second phase angle peak was appeared in the frequency 0.1 Hz. Then it can be inferred that the potential range of -0.4 V to 0 V was the optimal polarization potential region for DSS 2205 passivation in SCPS_{13.8}. However, in more alkaline solution, the stability of the passive film can be deteriorated, leading to a decrease of the corrosion resistance.

In addition, in SCPS_{13.8}, a straight line appeared in the low frequency range which indicates that the kinetics of the dissolution of the oxide film is limited by diffusion of the oxidation products. This is related to the increase of the solution pH. It suggests that the very alkaline environment could deteriorate the passivation process and make the worst protective passive films with the minimum radius of the semicircle arc. It can be found in Fig.4c and 4d that the impedance of Fe is obviously larger than that of DSS 2205 in the SCPS_{13.8}. This indicates that the passive film of pure Fe is better than DSS 2205. Compared with Fe, it takes more time for DSS 2205 to reach the steady state of the passivation. In addition, the passivation current of Fe is stable and has a wide passive range. As for 2205, the polarization current is unstable and this is related to the composition of the 2205. Then, it demonstrated that higher alkaline environment (pH >13) was not the optimal solution to improve the impedance and protective behavior of the DSS 2205. Compare these SCPS, it was found that the SCPS_{12.5} with the medium-high pH value was the best solution for the passivation of the DSS 2205, which could improve stability and corrosion resistance of the passive layer.

It was found that with the increase of the pH from 12.5 up to 13.8, the optimal formation potential will decrease from -0.1 V down to -0.4 V. This reflects that the passivation behavior is affected by the pH of the SCPS. As a contrast samples, the pure Fe was investigated as shown in Fig.4b and Fig.4d. It can be seen that the highest phase angle is -86° which indicated much stable and better protective behavior of the passive films. Furthermore, the broader peak range of phase angle is from 0.1 Hz to 10^3 Hz which shows the excellent passivation of the Fe. At the same time, the modulus $|Z|$ is in the range from $9.3 \times 10^5 \Omega \text{ cm}^2$ to $2.4 \times 10^6 \Omega \text{ cm}^2$. The pure Fe has a broad passive range and better passive behavior with good protective properties. It seems that pure Fe could display better protective behavior in very alkaline environment. Unlike pure Fe, DSS 2205 can be passivated well in the medium-high pH value in the passive range. The corrosion resistance of the films will weakened when the pH of the environment is above 13.

The two time constant equivalent circuit model (Fig.5), which can provide the best fitting results and the physical meaning of the relevant passivation process, has been selected for analyzing impedance spectra in this condition using the ZView software for the fitting process [39, 40]. As shown in Fig.5, the EEC contains solution resistance R_s connected in series with two time constants $R_1[Q_1(R_2Q_2)]$. This model assumed that the passive film on DSS 2205 was already formed. The passive film contains a porous layer on the outside, which is filled up with electrolyte. Moreover, it would be subjected to changes in the microstructural and electrical properties.

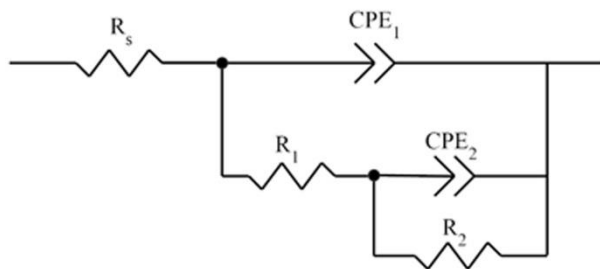


Figure 5. Electrical equivalent circuit (EEC) models for fitting the impedance spectra of the passive film on DSS 2205 in SCPS.

In this model, the passive film was not a homogeneous layer but rather a defective one. Here, CPE is used for the description of a non-ideal capacitance with varying n . The impedance of the CPE is given by:

$$CPE = Z(\omega) = Z_0 \cdot (i\omega)^{-n} \tag{1}$$

where Z^0 is the CPE constant. The factor n , which defined as a CPE power, is an adjustable parameter that always lies from -1 to 1. When $n = 1$, the CPE describes an ideal capacitance ($Z_0 = C$), when $n = -1$, the CPE symbolizes an ideal inductor ($Z_0 = L$), and when $n = 0$, CPE represent resistance ($Z_0 = R$). When $n = 0.5$, CPE depicts a Warburg impedance ($Z_0 = W$),

Table 1. Fitting parameters for the impedance spectra of DSS 2205 passivated 4 h at different polarization potentials in SCPS_{12.5} and SCPS_{13.3}.

Solution	$E(v.s.SCE)$	0.1 V	-0.1 V	-0.3 V	-0.5 V	-0.7 V
SCPS _{12.5}	$R_s (\Omega \text{ cm}^2)$	23.09	37.46	38.53	26.93	35
	$CPE_1 (\Omega^{-1} \text{ cm}^{-2} \text{ s}^{-n})$	4.92×10^{-5}	2.45×10^{-5}	2.97×10^{-5}	5.36×10^{-5}	4.89×10^{-5}
	n_1	0.94	0.94	0.94	0.90	0.91
	$R_1 (\Omega \text{ cm}^2)$	3.54×10^5	5.65×10^5	5.05×10^5	2.59×10^5	4.91×10^5
	$CPE_2 (\mu\Omega^{-1} \text{ cm}^{-2} \text{ s}^{-n})$	1.19×10^{-3}	1.91×10^{-5}	1.76×10^{-5}	9.14×10^{-5}	1.47×10^{-5}
	n_2	3.0	0.73	0.82	0.91	0.94
	$R_2 (\Omega \text{ cm}^2)$	1.99×10^5	4.58×10^5	5.0×10^5	1.32×10^5	1.54×10^6
SCPS _{13.3}	$R_s (\Omega \text{ cm}^2)$	33.66	42.64	38.63	36.48	35.17
	$CPE_1 (\Omega^{-1} \text{ cm}^{-2} \text{ s}^{-n})$	3.43×10^{-5}	2.13×10^{-5}	2.31×10^{-5}	3.76×10^{-5}	6.89×10^{-5}
	n_1	0.90	0.92	0.94	0.91	0.85
	$R_1 (\Omega \text{ cm}^2)$	9.23×10^4	2.02×10^5	1.9×10^5	1.67×10^5	9.84×10^4
	$CPE_2 (\mu\Omega^{-1} \text{ cm}^{-2} \text{ s}^{-n})$	4.89×10^{-4}	2.02×10^{-5}	2.6×10^{-5}	2.54×10^{-4}	1.26×10^{-5}
	n_2	1.22	1.39	0.63	1.01	0.71
	$R_2 (\Omega \text{ cm}^2)$	4.17×10^3	8.93×10^3	3.46×10^5	2.83×10^4	2.70×10^5

Table 1 shows the fitting parameters for the impedance spectra of DSS 2205 polarization 4 h at different polarization potentials in SCPS_{12.5} and SCPS_{13.3} based on the equivalent circuit in Fig.5. It was found that, the film resistance R_1 in SCPS_{12.5} decreased with the polarization potential decrease, which reflects the protective property of the film become worse. However, at the potential 0 V, the R_1 was $1.43 \times 10^6 \Omega \text{ cm}^2$ which was the maximum. As for SCPS_{13.3}, it can be seen that the R_1 is small than

that of SCPS_{12.5} at the same formation potential. It indicated that the value of R_1 will decrease with the increase of the SCPS pH value. Also, when the polarization potential is negative than -0.6 V, the R_1 decreases sharply. With the decrease of formation potential to more negative in the passive range, the CPE_1 which represents the surface heterogeneity decreases from 0.2 V ($4.78 \times 10^{-5} \mu\Omega^{-1} \text{cm}^{-2} \text{s}^{-n}$) down to -0.1 V ($-2.45 \times 10^{-5} \mu\Omega^{-1} \text{cm}^{-2} \text{s}^{-n}$), then increase from -0.1 V to -0.8 V ($6.84 \times 10^{-5} \mu\Omega^{-1} \text{cm}^{-2} \text{s}^{-n}$), represent the defects in the passive film. The value of the exponent n is about 0.88-0.94 in the passive region, which shows that the CPE_1 has the good capacitive behavior. The CPE_2 value is very close to the typical double layer capacitance. In general, the CPE_2 decreases as the polarization potential shift to more negative. The charge transfer resistance R_2 , which is seems to be dependent on the E_{corr} of the passive films, varies with film formation potential, with the largest value in -0.2 V to -0.4 V range. This exhibits a slow rate of reactions taking place at the film/electrolyte interface, which means that the passive film formed near the E_{corr} of the passive films are more protective. It can be inferred that the best potential will shift negative at higher alkaline environment.

The polarization resistance (R_p) could reflect the corrosion resistance of the passive film [41]. High R_p indicates good protective ability in alkaline environments. According to the ECC, R_p can be calculated by the $1/R_p = (1/R_1) + (1/R_2)$. The R_p data was calculated as shown in Fig.6. It can be seen that the R_p obtained in SCPS_{13.3} is small than that of SCPS_{12.5}. With the increase of the formation potential from -0.8 V to 0.2 V, R_p decreases in the range of -1.0 V to -0.5 V. Then, the R_p increases from -0.5 V to -0.2 V, which is also the potential region of E_{corr} of the passive film. When the formation potential surpasses -0.2 V, the R_p will decrease slowly and keep constant after 0 V. It need to point out that there are many factors affect the value of R_p . Obviously, the R_p obtained in the SCPS_{12.5} is large. Although fluctuation can be found for R_p in the $R_p \sim V$ curves as shown in Fig.6, the shape of the $R_p \sim V$ curve is almost the same, which suggests the consistent change trend of R_p . It can be seen that better corrosion resistance of the passivation will be formed when the polarization potential is close to the E_{corr} of the stable passive layers, which is near -0.1 V to -0.3 V.

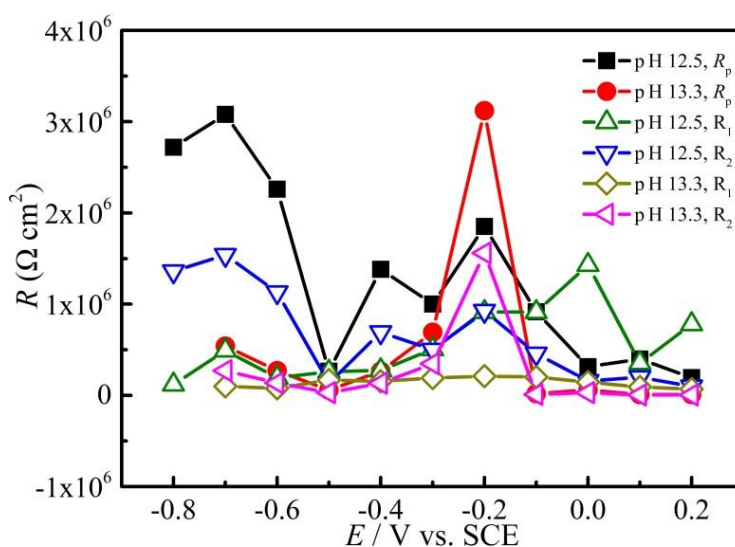


Figure 6. R_p change plot as a function of passive film formation potential in different SCPS.

3.4 Electrochemical properties of the passive films on DSS 2205

Fig.7a, b is the Tafel plot of the DSS 2205 passivated 4h at different potential in SCPS. As can be seen in Fig.7a, in the SCPS_{12.5}, most of the passive film covered DSS 2205 showed a broader passive range from about -0.8 V to 0.4 V. After 0.4 V, the passive film begins to breakdown and pitting corrosion initiates. In addition, the formation potential also affects the corrosion potential of the passive films, which can be checked by the changes of the E_{corr} in Fig.7a. In the most case, no pitting corrosion was observed. It can be found in Fig7a that with the increase of the polarization potential from -0.8 V to 0.2 V, the E_{corr} shifts from -0.95 V to -1.03 V. The E_{corr} rarely changes and the i_{corr} decreases with the increase of the polarization potential. Two oxidation peaks were observed at -0.85 V and -0.44 V, which is corresponding to the Fe, Cr oxidation reactions.

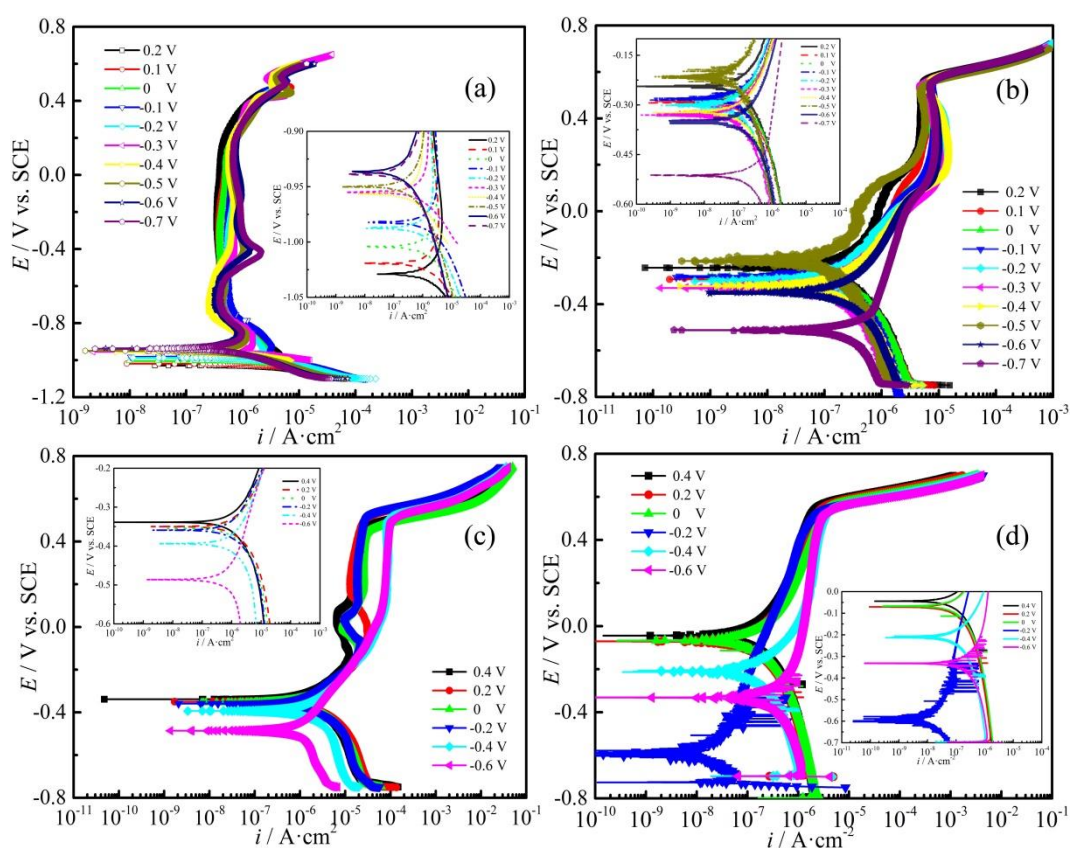


Figure 7. Tafel plots of DSS 2205 passivated at different potential at 0.1667 mV/s in the solution (a) 4h, SCPS_{12.5}, (b) 4h, SCPS_{13.3}, (c) 24h, SCPS_{13.8}. (d) pure Fe, 24 h, SCPS_{13.8}.

Compared with SCPS_{12.5}, the breakdown potential of the passive films in the SCPS_{13.3} is obvious as seen in Fig.7b. It was observed that the E_{corr} shifts to positive than that in SCPS_{12.5} with the increase of the polarization potential. No obvious redox peaks was found in the plots. As shown in Fig.7c, in the SCPS_{13.8}, the corrosion potential positively shifts largely. The E_{corr} was positive shift to -0.35 V, which shows the good corrosion resistance of the passive films. However, the breakdown potential of the films was 0.4 V. The corrosion current increases which is associated with the high pH

value of the SCPS. The shape of the Tafel plot at any polarization potentials is similar though some differences exist related to redox peak. In SCPS_{13.8}, the passive film was poorly formed and has less protective ability. This is because that the high alkaline SCPS is beneficial to the development of metastable pits which generated the poor quality of the passive film. Thus, it can be concluded that the formation process of the passive film is a dynamic process [42, 43]. Proper pH value is necessary for formation of the passive films with good protective ability.

As shown in Fig.7d, the E_{corr} of the passivated Fe shifts to positive from -0.5 V to about 0 V with the increase of the formation potential. This confirmed that the passivation property of the Fe is greatly affected by the applied formation potential. As for the passivated Fe, no current peaks appeared which is different from that of DSS 2205. In the passive range of DSS 2205, there have some current peaks corresponding to the oxidation reaction of the component in DSS 2205. This indicated that there has the optimal potential for passivation the DSS 2205. The pH and formation potential both affect the passivation process.

Based on the analysis of Tafel plots, E_{corr} as a function of polarization potential was supplied in Fig.8a. It can be seen that the E_{corr} in SCPS_{12.5} is low and stable. However, when the pH is above 13, the E_{corr} is more positive with a fluctuation between -0.4 V and -0.2 V. With the increase of the formation potential from -0.8 V to 0.2 V, on the whole, the E_{corr} increases. Although the E_{corr} was not stable and easily varied in potentiodynamic technique, the results still could reflect the formation behavior of the passive film on the DSS 2205 surface.

The electrochemical capacitance of the passive film/electrolyte interface was measured as a function of the polarization potential to assess the semiconducting properties of the passive films formed on DSS 2205. The relationship between capacitance and the polarization potential is given by the Mott-Schottky equation [44], which describes the potential dependence of the space charge capacity, C , of a semiconductor electrode under depletion condition:

$$\frac{1}{C^2} = \pm \frac{2}{e \cdot N \cdot \epsilon \cdot \epsilon_0} \left(E - E_{\text{FB}} - \frac{kT}{e} \right) \quad (2)$$

where the negative sign is for p-type and the positive sign for n-type conductivity, e the electron charge, N charge carrier density, the donor density for n-type or the acceptor density for p-type semi- conductors, ϵ_0 the vacuum permittivity, ϵ the relative dielectric constant of the semiconductor, k Boltzmann's constant and T absolute temperature, E the applied electrode potential and E_{FB} the flat band potential. The Mott-Schottky plots of DSS 2205 in SCPS solution is shown in Fig.8b. It displays the C^2 vs. E curve for the passive film formed on DSS 2205 at different potentials within the passive region. It demonstrates that the passive film of DSS 2205 displays the oxide behavior as the n-type semiconductor when the polarization potential is below -0.2 V. However, when the polarization potential is above -0.1 V, the passive film could display both n-type and p-type semiconductor behavior according to the potential. The decrease of capacitance with the polarization potential is attributed to the increase of the electron depleted layer and a diminishing number of charge carriers [45, 46]. This phenomenon indicates a change in electronic properties of the passive film, and is associated with the increase in the conductivity of the film [47].

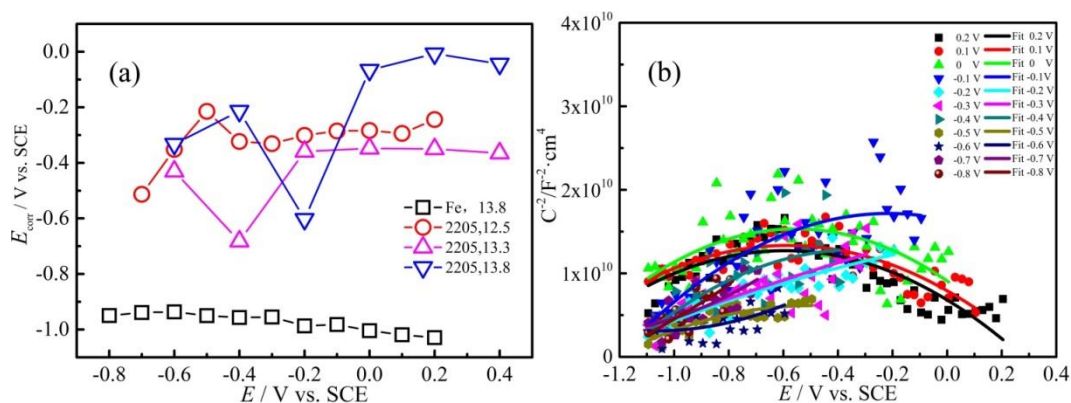


Figure 8. (a) E_{corr} plot as a function of the polarization potential in different SCPS, (b) Mott Schottky of DSS 2205 from polarization potential to -1.0 V_{SCE} at a step rate of 25 mV/s, 5000 Hz, 25°C, in SCPS_{12.5}.

The values of N_D (N doping density), N_A can be determined from the slope of the experimental C^{-2} vs. E . The charge carrier density N can be obtained by calculation the slopes of the linear portion of the C^{-2} vs. E [48], from the equation (3):

$$N = \frac{2}{m \cdot e \cdot \epsilon \cdot \epsilon_0} \quad (3)$$

where m is the slope of the Mott-Schottky plot in the linear-region of interest, e is the electron charge, ϵ the relative dielectric constant of the semiconductor, ϵ_0 the vacuum permittivity, the value is $8.85 \times 10^{-12} \text{ F m}^{-1}$. Based on the calculated results, the values of N are in the range of 10^{20} - 10^{22} cm^{-3} , which are consistent with the reported values for the passive film of steels. Moreover, the values of N_D and N_A decrease with the increase of potentials. Therefore, passive films of DSS 2205 formed at low passive potentials have more disordered structures and higher defect densities than those formed at higher passive potentials.

4. CONCLUSIONS

The electrochemical behavior of DSS 2205 in SCPS under anoxic condition was evaluated mainly by EIS technique. The main conclusions can be obtained as follows: The DSS 2205 exhibits well passive behavior in SCPS with passive region from -0.4 V to 0.4 V vs. SCE. The formation and protective properties of the passive film are greatly influenced by the pH and polarization potential. With the increase of pH from 12.5 to higher, the corrosion resistance of the passive film decreased. As the pH increases and polarization potential shifts to more negative, the time (T_s) for polarization current to reach stable will be prolonged. The R_p formed in SCPS_{12.5} is larger than that of SCPS_{13.3}, which indicated that the passive film formed in SCPS_{12.5} was thicker than that of SCPS_{13.3}. The passive film displays the behavior of n-type semiconducting when the polarization potential is below -0.2 V. It was found that the highest polarization potential is not corresponding to the best impedance value. The optimal formation potential is related to the E_{corr} of the formed passive films. The potential which is between 300 mV positive and 100 mV negative to E_{corr} of the passive film is the optimal formation

potential for passivation of the DSS 2205 in SCPS, which is usually in the range of 0 mV to -400 mV vs. SCE.

ACKNOWLEDGEMENTS

The authors gratefully acknowledge financial support from the National Natural Science Foundation of China (No. 51679076, 51605137, 51301061).

References

1. X. Feng, X. Lu, Y. Zuo, D. Chen, *Corros. Sci.*, 82 (2014) 347.
2. M. Liu, X. Cheng, X. Li, P. Yue, J. Li, *J. Mater. Eng. Perform.*, 25 (2016) 4967.
3. M. Behzadnasab, S.M. Mirabedini, M. Esfandeh, R.R. Farnood, *Prog. Org. Coat.*, 105 (2017) 212.
4. J. Chen, *Int. J. Electrochem. Sci.*, 12(2017) 1348.
5. M. Mohammadi, L. Choudhary, I.M. Gadala, A. Alfantazi, *J. Electrochem. Soc.*, 163 (2016) C883.
6. J. Lv, T. Liang, C. Wang, T. Guo, *J. Alloys Compd.*, 658 (2016) 657.
7. F. Mao, C. Dong, S. Sharifi-Asl, P. Lu, D.D. Macdonald, *Electrochim. Acta*, 144 (2014) 391.
8. Y. Zhang, M. Urquidi-Macdonald, G.R. Engelhardt, D.D. Macdonald, *Electrochim. Acta*, 69 (2012) 1.
9. S. Wang, Q. Ma, Y. Li, *Mater. Des.*, 32 (2011) 831.
10. C.B. Zheng, L. Cai, Z.J. Tang, X.L. Shen, *Surf. Coat. Technol.*, 287 (2016) 153.
11. S.M. Alvarez, A. Bautista, F. Velasco, *Corros. Sci.*, 53 (2011) 1748.
12. G.L. Song, K.A. Unocic, *Corros. Sci.*, 98 (2015) 758.
13. F. Mao, C. Dong, D.D. Macdonald, *Corros. Sci.*, 98 (2015) 192.
14. W. Dec, M. Mosialek, R.P. Socha, M. Jaworska-Kik, W. Simka, J. Michalska, *Electrochim. Acta*, 212 (2016) 225.
15. J.C. Galván, M.T. Larrea, I. Braceras, M. Multigner, J.L. González-Carrasco, *J. Alloys Compd.*, 676 (2016) 414.
16. L. Zhang, A. Ma, J. Jiang, D. Song, D. Yang, J. Chen, *Surf. Coat. Technol.*, 232 (2013) 412.
17. W. Kuang, J.A. Mathews, M.L. Taylor, D.D. Macdonald, *Electrochim. Acta*, 136 (2014) 493.
18. R.G. Duarte, A.S. Castela, R. Neves, L. Freire, M.F. Montemor, *Electrochim. Acta*, 124 (2014) 218.
19. P. Lu, B. Kursten, D.D. Macdonald, *Electrochim. Acta*, 143 (2014) 312.
20. M. Criado, I. Sobrados, J. Sanz, J.M. Bastidas, *Surf. Coat. Technol.*, 258 (2014) 485.
21. M. Cabrini, S. Lorenzi, T. Pastore, *Electrochim. Acta*, 124 (2014) 156.
22. J.M. Deus, B. Díaz, L. Freire, X.R. Nóvoa, *Electrochim. Acta*, 131 (2014) 106.
23. H. Luo, H. Su, C. Dong, K. Xiao, X. Li, *Constr. Build. Mater.*, 96 (2015) 502-507.
24. S. Sharifi-Asl, F. Mao, P. Lu, B. Kursten, D.D. Macdonald, *Corros. Sci.*, 98 (2015) 708-715.
25. S. Fajardo, D.M. Bastidas, M. Criado, J.M. Bastidas, *Electrochim. Acta*, 129 (2014) 160.
26. S. Sharifi-Asl, M.L. Taylor, Z. Lu, G.R. Engelhardt, B. Kursten, D.D. Macdonald, *Electrochim. Acta*, 102 (2013) 161.
27. S. Sharifi-Asl, D.D. Macdonald, A. Almarzooqi, B. Kursten, G.R. Engelhardt, *J. Electrochem. Soc.*, 160 (2013) C316.
28. D. Addari, B. Elsener, A. Rossi, *Electrochim. Acta*, 53 (2008) 8078.
29. Y. Wang, Y. Zuo, X. Zhao, S. Zha, *Appl. Surf. Sci.*, 379 (2016) 98.
30. Y. Wang, X. Cheng, X. Li, *Electrochem. Commun.*, 57 (2015) 56.
31. C.Q. Ye, R.G. Hu, S.G. Dong, X.J. Zhang, R.Q. Hou, R.G. Du, et al., *J. Electroanal. Chem.*, 688 (2013) 275.
32. Y. Wang, X. Cheng, X. Li, *Electrochem. Commun.*, 57 (2015) 56.

33. F. Tang, X. Cheng, G. Chen, R.K. Brow, J.S. Volz, M.L. Koenigstein, *Electrochim. Acta*, 92 (2013) 36.
34. H. Luo, S. Gao, C. Dong, X. Li, *Electrochim. Acta*, 135 (2014) 412.
35. D. Han, Y.M. Jiang, C. Shi, B. Deng, J. Li, *J. Mater. Sci.*, 47 (2011) 1018.
36. S.M. Abd El Haleem, S. Abd El Wanees, A. Bahgat, *Corros. Sci.*, 75 (2013) 1.
37. A. Fattah-alhosseini, S. Vafaeian, *Appl. Surf. Sci.*, 360 (2016) 921.
38. H. Kahn, A.H. Heuer, G.M. Michal, F. Ernst, R. Sharghi-Moshtaghin, Y. Ge, P.M. Natishan, R.J. Rayne, F.J. Martin, *Surf. Eng.*, 28 (2013) 213.
39. L. Jinlong, L. Tongxiang, W. Chen, D. Limin, *J. Electroanal. Chem.*, 757 (2015) 263.
40. M. Naghizadeh, M.H. Moayed, *Corros. Sci.*, 94 (2015) 179-189.
41. R. Feng, J. Beck, M. Ziomek-Moroz, S.N. Lvov, *Electrochim. Acta*, 212 (2016) 998.
42. K. Karadakis, V.J. Azad, P. Ghods, O.B. Isgor, *J. Electrochem. Soc.*, 163 (2016) C306-C315.
43. P. Lu, G.R. Engelhardt, B. Kursten, D.D. Macdonald, *J. Electrochem. Soc.*, 163 (2016) C156.
44. H. Luo, C.F. Dong, X.G. Li, K. Xiao, *Electrochim. Acta*, 64 (2012) 211.
45. S. Vafaeian, A. Fattah-alhosseini, M.K. Keshavarz, Y. Mazaheri, *J. Alloys Compd.*, 677 (2016) 42.
46. R.D. Moser, P.M. Singh, L.F. Kahn, K.E. Kurtis, *Corros. Sci.*, 57 (2012) 241-253.
47. M.S. Anwar, B. Fadillah, A. Nikitasari, S. Oediyani, E. Mabruri, *Procedia Eng.*, 171 (2017) 517.
48. H. Luo, H. Su, C. Dong, X. Li, *Appl. Surf. Sci.*, 400 (2017) 38.

© 2017 The Authors. Published by ESG (www.electrochemsci.org). This article is an open access article distributed under the terms and conditions of the Creative Commons Attribution license (<http://creativecommons.org/licenses/by/4.0/>).